JOURNAL OF GEOPHYSICAL RESEARCH, VOL. 113, D14106, doi:10.1029/2007JD009230, 2008

MJO and its relationship to ENSO

Youmin Tang[1] and Bin Yu[2]

Received 27 July 2007; revised 19 December 2007; accepted 19 February 2008; published 17 July 2008

[1] In this study, we detected the spatial and temporal characteristics of Madden-Julian Oscillation (MJO) using zonal winds at the surface and outgoing long-wave radiation (OLR) from the NCEP-NCAR (U.S. National Center of Environmental Prediction-National Center for Atmospheric Research) reanalysis product from 1981–2003. The results show that MJO activity, represented by these two variables, has large variances around 10° off the equator and over the near-equatorial western Pacific. One central issue addressed in this study is MJO-ENSO (El Niño and Southern Oscillation) relationship. It has been found that there exists a statistically significant relationship between MJO in spring-summer and ENSO in autumn-winter. The relationship of MJO-ENSO is nonlinear in nature and has a decadal variation. A much stronger statistical relationship of MJO-ENSO was found in the 1990s as compared to that in the 1980s. These findings were further verified using ECMWF (European Center for Medium-Range Weather Forecasts) reanalysis product. The potential mechanisms responsible for MJO-ENSO relationship are also discussed.

Citation: Tang, Y., and B. Yu (2008), MJO and its relationship to ENSO, *J. Geophys. Res.*, *113*, D14106, doi:10.1029/2007JD009230.

1. Introduction

[2] MJO is the dominant component of the intraseasonal (30–90 d) variability in the tropical atmosphere. It is typically characterized by eastward-traveling circulation cells moving along the equatorial plane, observed mainly over the Indian Ocean and the western Pacific Ocean. The MJO involves variations in a variety of fields such as wind, sea surface temperature (SST), cloudiness, rainfall, and OLR. Spectral analyses generally indicate a peak of their energy densities around 30- to 90-day period and a distinctive wave number one structure in the zonal direction.

[3] MJO has significant impact on global weather and climate anomalies. The active phase of the MJO often provides the environment for high-impact weather events (e.g., tropical cyclones; monsoon precipitation anomalies). Observational and theoretical work has also shown that MJO may have a significant influence on ENSO, and may thus have important implications for climate prediction, especially for the prediction of ENSO [e.g., *Lau et al.*, 1989; *McPhaden et al.*, 2006; *Hendon et al.*, 2007; Y. Tang and B. Yu, An analysis of nonlinear relationship between the MJO and ENSO, submitted to *Journal of the Meteorological Society of Japan*, 2008]. Therefore it has been of great interest to investigate the connection of MJO-ENSO. It was argued that the MJO can impact ENSO as a stochastic forcing (SF) like westerly wind burst (WWB) (MJO is substantially different from WWB, and has a much larger spatial and temporal scales and much less occurrence frequency than WWB), which often occurs over the western equatorial Pacific during the onset of some El Niño events such as 1982/1983 and 1997/1998 [*Yu and Rienecker*, 1998; *Harrison and Geise*, 1991]. Indeed, the role of SF on ENSO cycle has been addressed during TOGA (Tropical Ocean-Global Atmosphere), especially since the late 1990s. Many studies show that the effects of realistic SF applied to a hybrid or an intermediate coupled model in a regime that would otherwise be periodic are sufficient to produce irregularity generally consistent with observed ENSO signals [*Blanke et al.*, 1997; *Eckert and Latif*, 1997; *Kleeman and Moore*, 1997; *Moore and Kleeman*, 1999; *Zavala-Garay et al.*, 2005]. It has also been observed that anomalous SF activity in the western Pacific often proceeds ENSO events and could trigger or modify ENSO events by downwelling Kelvin waves [*Webster and Palmer*, 1997; *McPhaden*, 1999].

[4] Previous observation and modeling studies generally indicated that MJO activity often precedes El Niño, however the statistically significant relationship between them has not been well identified [e.g., *Slingo et al.*, 1999; *Hendon et al.*, 1999; *Kessler*, 2001]. One central question here is whether the link between MJO and ENSO is random in nature, thereby no statistically significant relationship existing, or nonlinear thus widely used linear statistical techniques being invalid? Recently, *McPhaden et al.* [2006] and *Hendon et al.* [2007] found that MJO-ENSO relationship has seasonal dependence. Further Tang and Yu (submitted manuscript, 2008) demonstrated that the relationship is nonlinear in nature. These studies show significantly lagged correlations between MJO and ENSO indices.

[1]Environmental Science and Engineering, University of Northern British Columbia, Prince George, British Columbia, Canada.
[2]Climate Research Division, Environment Canada, Toronto, Ontario, Canada.

0148-0227/08/2007JD009230$09.00

[5] In this study, we will further explore the relationship of MJO-ENSO using different MJO indices, with emphases on its nonlinear, seasonal and decadal dependence. This paper is structured as follows: section 2 briefly describes the data and analysis techniques. Section 3 detects the ENSO signals. Section 4 presents two estimates of MJO activity. In section 5, we present a detailed analysis of MJO-ENSO relationship including its seasonal dependence, decadal variation and nonlinearity, followed by conclusion and discussion in section 6.

2. Data and Analysis Techniques

2.1. Data

[6] The zonal winds at the surface and OLR were used to diagnose intraseasonal and MJO activity. The data were obtained from daily NCEP-NCAR reanalysis product from January 1981 to December 2003 (http://www.cdc.noaa.gov/cdc/data.ncep.reanalysis.html). We analyzed the data after 1979 considering that the introduction of satellite data in 1979 may bring some effects on the diagnosis. The NCEP-NCAR reanalysis product has a various resolution for different variables with $2.5^\circ \times 2.5^\circ$ for zonal winds and $1.88^\circ \times 1.89^\circ$ for OLR. For further verification, we also used ERA-40 $2^\circ \times 2^\circ$ daily reanalysis zonal winds at the surface from 1981 to 2001 [*Uppala et al.*, 2005]. Observed SST is from Reynolds $2^\circ \times 2^\circ$ monthly data set [*Reynolds and Smith*, 1994]. The SST is temporally interpolated to daily values using a linear scheme as discussed by *Zavala-Garay et al.* [2005]. The climatology annual cycle for each calendar day is computed, and then subtracted from the raw data for each data set.

[7] The domain of interest was spanned in the tropical Pacific from 15°S to 15°N, and 120°E to 70°W. We focus on the tropical Pacific Ocean, since considerable evidences show that it is the MJO activity in the tropical Pacific, in particular in the western Pacific, that plays a critical role in influencing ENSO [e.g., *Kessler*, 2001; *McPhaden et al.*, 2006; *Hendon et al.*, 2007; Tang and Yu, submitted manuscript, 2008].

2.2. Analysis Techniques

[8] The empirical orthogonal function (EOF) is a widely used method to study a high-dimensional data set in a low-dimensional space. It is capable of using few leading modes to describe dominant structures that explain the majority of overall variances. However, EOF only depicts stationary modes that are unable to interprete propagation properties of the data set, thus the time-lagged extended EOF (EEOF) analysis and Complex EOF (CEOF [e.g., *Barnett*, 1983]) are employed in this study.

[9] EEOF constitutes an extension of the traditional EOF technique to deal not only with spatial- but also with temporal correlations. It uses an extended matrix to compute covariance. The extended matrix is composed of a series of time-lagged data matrix, generated by the raw data matrix. Consider a space-time data matrix M with P spatial grids and N samples in time. Sliding a time window of length W over N ($W < N$) produces a time-lagged matrix. Moving the window forward and repeating the above process gets the second time-lagged matrix, and so forth. Therefore the EEOF provides not only eigenvectors but also the temporal evolutions of the eigenvectors. A detailed description of EEOF is discussed by *Tangang et al.* [1998].

[10] CEOF analysis has been used in the past to detect wave propagating. Like EEOF, CEOF is another derivative of EOF. In CEOF, the covariance is computed using a complex matrix. The complex matrix $\mathbf{U}$ should be constructed with the real data matrix $\mathbf{M}$ using a Hilbert Transform, i.e., $\mathbf{U} = \mathbf{M} + \tilde{\mathbf{M}}$, where $\tilde{\mathbf{M}}$ is the imaginary part, generated by the Hilbert Transform as below,

$$\tilde{\mathbf{M}}(t) = \sum_{l=-L}^{L} \mathbf{M}(t-l)h(l) \tag{1}$$

where

$$h(l) = \begin{cases} \dfrac{2}{l\pi}\sin^2(l\pi/2) & \text{if } l \neq 0; \\ 0, & \text{if } l = 0. \end{cases}$$

[11] Ideally $L = \infty$ in (1). In this study L is set to 7 as given by *Barnett* [1983] and *Zavala-Garay et al.* [2005].

[12] Two important measures are often used in CEOF: amplitude function $\mathbf{R}$ and phase function $\boldsymbol{\theta}$. The former represents the anomalous amplitude of an eigenvector whereas the latter depicts its propagation. Denote by B an eigenvector, $\mathbf{R}$ and θ are respectively defined as below

$$\mathbf{R} = \mathbf{B} \times \mathbf{B}^*; \boldsymbol{\theta} = \arctan\left[\frac{Im\mathbf{B}}{Re\mathbf{B}}\right] \tag{2}$$

where $\mathbf{B}^*$ is conjugate of B.

[13] We also use two other statistical methods, singular value decomposition (SVD) and neural network (NN), to detect statistical relationship between variables. The former is a linear technique while the latter is nonlinear. In general, SVD captures optimally coupled spatial structures by maximizing the covariance between various possible patterns [*Bretherton et al.*, 1992]. The detailed formulation of the NN model is described by *Tang et al.* [2001].

3. ENSO Signals

[14] Since the ocean has a long-term memory in the coupled atmosphere-ocean system, the oceanic contribution is often the source of the low-frequency atmospheric variability. On the basis of *Hasselmann's hypothesis* [1976], surface forcing can be decomposed into low-frequency slow components plus a residual, which primarily consists of random forcing representing fast atmospheric transients. As discussed by *Zavala-Garay et al.* [2005], we refer to the oceanic contribution as the ENSO-contribution and the residual as "non-ENSO" contribution.

[15] We measure respectively the oceanic contribution to surface forcing by two statistical models, linear SVD and nonlinear NN. The season cycle was removed from data sets prior to performing SVD and NN analyses. It was found that the existing relationship between surface forcing and SST anomalies is essentially linear, and the nonlinear model shows little improvement. Thus we only present the results from the SVD method for simplicity in following.

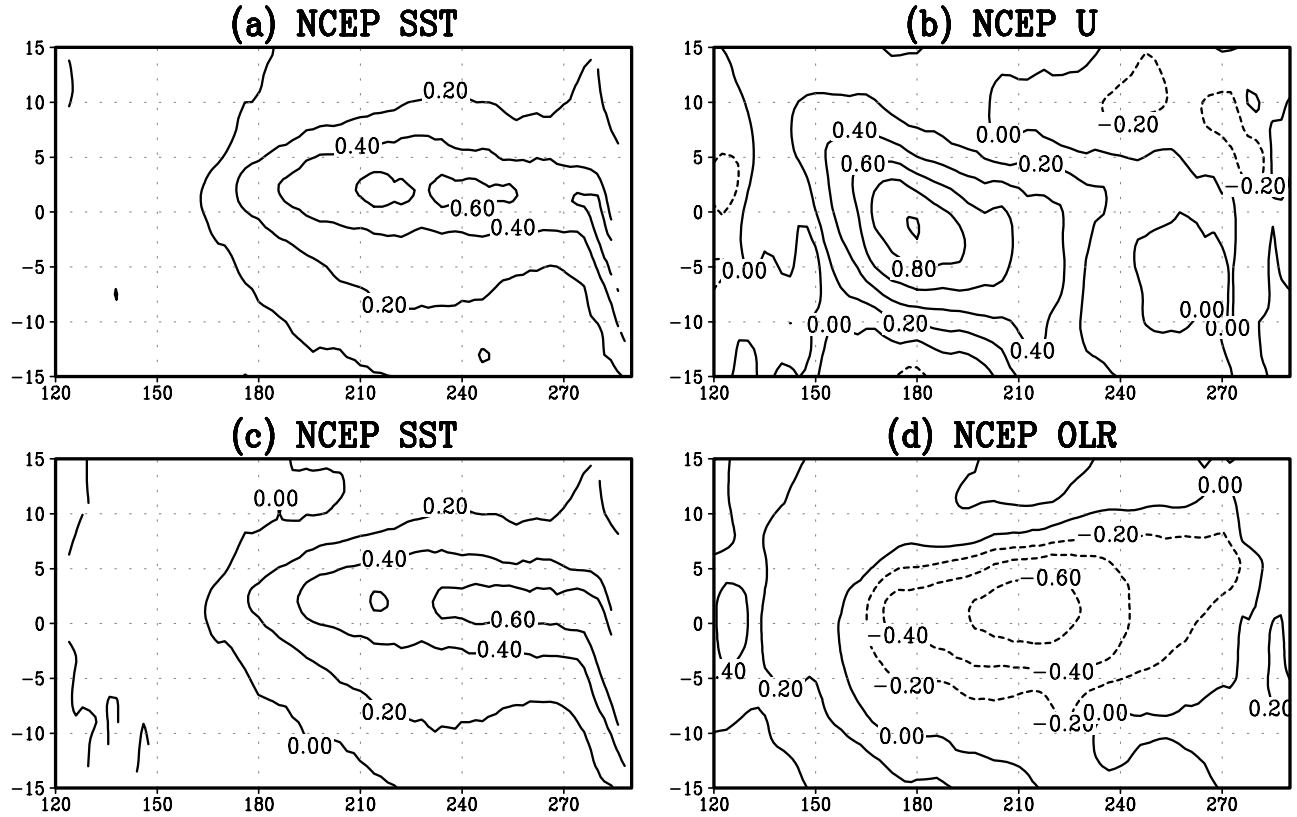

Figure 1. Leading SVD mode for (a and b) SST-zonal winds, and for (c and d) SST-OLR. The first modes account for 80.4% and 87.5% of total variance respectively. Unit is m s^{-1} for zonal wind, °C for SST and W/m^2 for OLR. The contour interval is 0.2.

[16] Figures 1a and 1b show the first singular vector for SST and zonal winds at the surface, accounting for 80.4% of total variance. In this mode, the warm (cold) water present in the equatorial eastern Pacific Ocean corresponds with large westerly (easterly) wind anomalies over the equatorial central Pacific. This is a typical ENSO-like structure, suggesting a strong coupling between atmosphere and ocean in the equatorial and central Pacific Ocean that can be described by the delayed oscillator theory [e.g., *Tang and Hsieh*, 2002].

[17] Figures 1c and 1d are the first singular vector for SST and OLR, accounting for 87.5% of total variance. The strong warming (cooling) in the eastern Pacific during El Niño (La Niña) leads to strong ascending (descending) motions where there is a large reduction (increase) in OLR, in association with a typically anomalous Walker circulation. At the region off the equator, the convergence (divergence) produces rise (subsidence) and cloudy (clear) sky conditions, also resulting in a decrease (increase) in OLR. Thus a physical relationship between SST and tropical convection anomalies is clearly shown here.

[18] To identify ENSO-like signal in surface forcing, we calculate the power spectrum at the ENSO frequencies. We define the total power at ENSO frequencies as the integral of the spectral density in the window with periods of 3–7 years as given by *Zavala-Garay et al.* [2005]. Figure 2 shows respectively the power spectrum at ENSO frequencies for the raw zonal winds (Figure 2a), for those estimated by the SVD model (Figure 2b) and for the residual (Figure 2c). ENSO signal is mainly present in the western-central equatorial Pacific in zonal winds. Comparing Figures 2a and 2b reveals that the SST contribution from the SVD model explains most of ENSO signal. However, there is still relatively weak ENSO signal in the residual field, probably excited by stochastically induced Kelvin waves and Rossby waves. A similar picture emerges with OLR (not shown).

4. MJO Signals

[19] Like the power definition for ENSO, we define the total power at MJO frequencies as the integral of the spectral density in the window with periods 30–90 d. Figure 3 shows the power spectrum at MJO frequencies for zonal winds. The strong MJO signal appears in the off-equatorial region and in the western Pacific, whereas there is weak MJO signal in the central and eastern equatorial Pacific (Figure 3a). The power structure for MJO is different from that for ENSO. In addition, A comparison between Figures 3a and 3c reveals that the MJO signal is mainly contributed by atmospheric internal activities. The oceanic contribution (ENSO) to MJO is very weak (Figure 3b). These features were also seen in the spectral analysis of the OLR (not shown).

[20] The spatial and temporal characteristics of MJO can also be identified by employing a CEOF analysis. Shown in Figure 4 is the spatial amplitude function of CEOF for zonal winds and OLR. A bandpass filter of 30–90 d^{-1} was

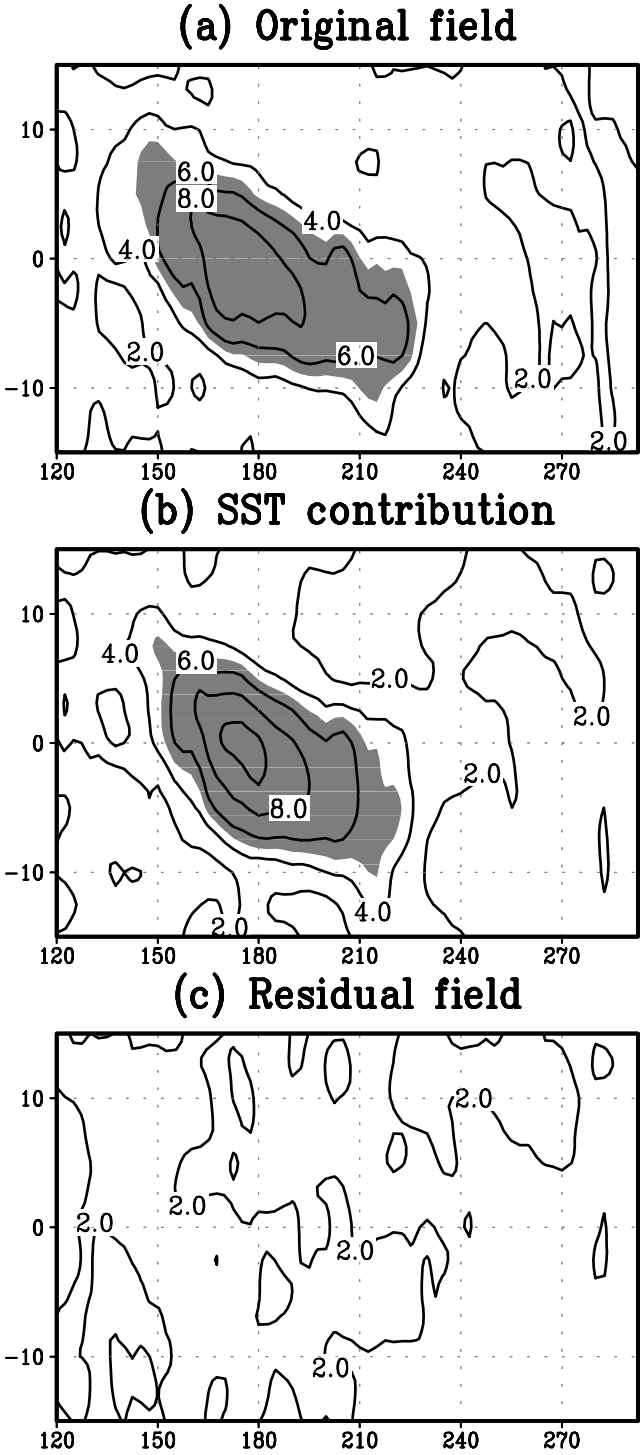

Figure 2. Spectrum power of ENSO frequency of 3–7 years in the NCEP reanalysis for zonal winds at the surface, (a) original winds; (b) estimated winds by the statistical model; (c) residual field between original and estimated winds. The unit is m^2 s^{-2}. Shaded are regions where the power has magnitude greater than 4, which was arbitrarily chosen for a good presentation. The contour interval is 2.

applied here prior to the CEOF analysis, so that only intraseasonal signals are kept in CEOF modes. The first CEOF modes explain 33% and 35% of total variance for zonal winds and OLR, respectively, both showing the strong MJO signal in the off-equatorial region of the western Pacific as noted in Figure 3.

[21] The strong MJO signal in the off-equatorial region as seen from Figures 3 and 4 suggests that the MJO activity

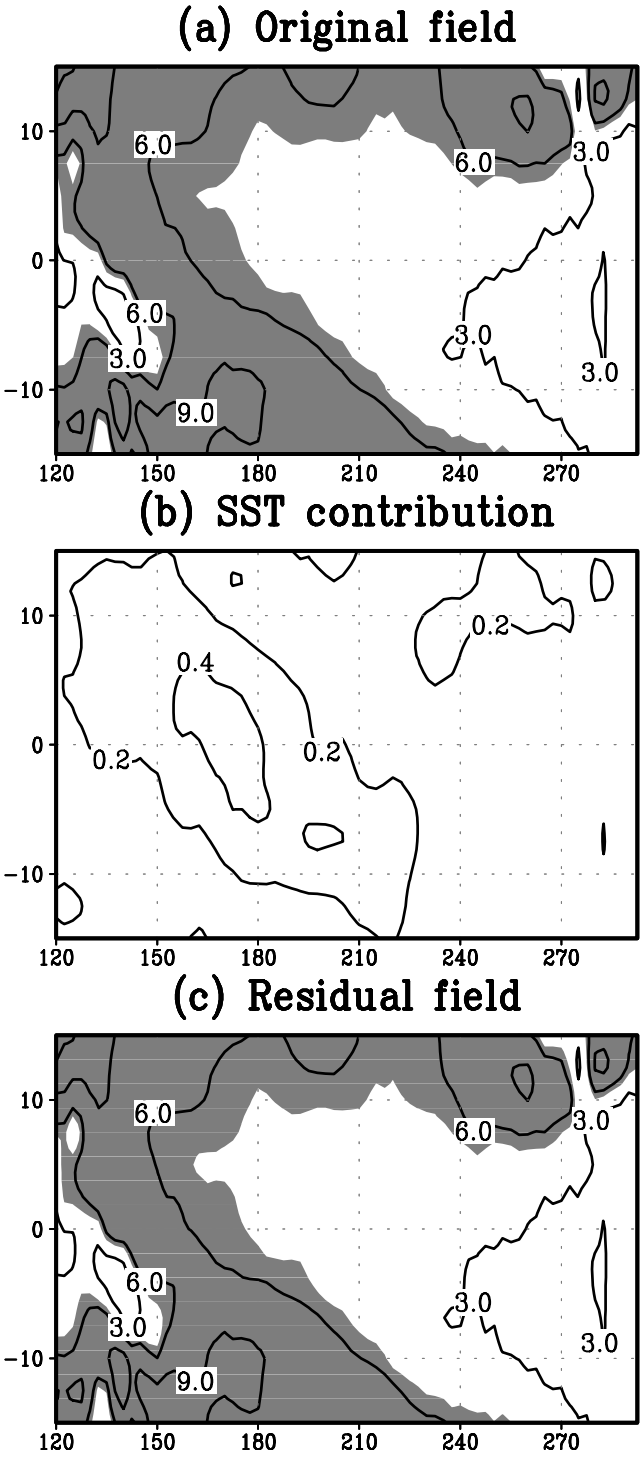

Figure 3. Spectrum power of MJO frequencies of 30–90 d for zonal winds (a) original winds, (b) estimated winds by statistical model, and (c) residual field between original and estimated winds. The unit is m^2 s^{-2}. The magnitude of the power over 5 is shaded. The interval level is 0.2 for Figure 3b and 3 for others.

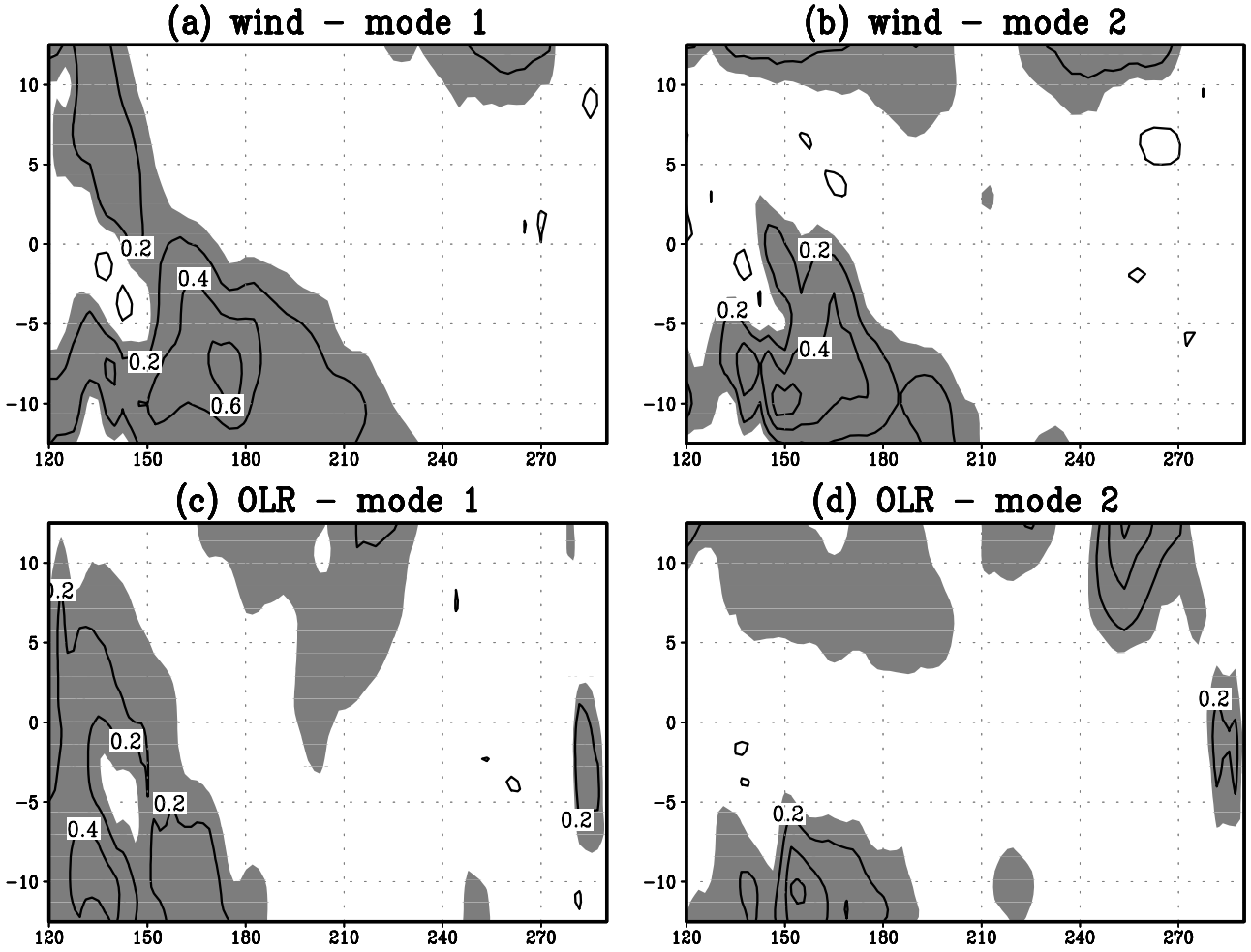

Figure 4. First two leading CEOF spatial amplitude modes for (a and b) zonal winds and (c and d) OLR. Shaded are regions where the value is over 0.1. The unit is $m^2\ s^{-2}$ for zonal wind and W/m^2 for OLR. The contour interval is 0.2.

represented by zonal winds at the surface and OLR is not spatially symmetric about the equator. It should be noted that there are several other important features for MJO, though some of them were directly diagnosed in this study: (1) MJO is a three-dimensional entity and has a varied representation by different variables. For example, in boreal winter the maximum variance of MJO activity occurs in the equatorial eastern Pacific in zonal winds at 200 hPa but in around 10°S of the western Pacific in zonal winds at 850 hPa and precipitation (H. Lin et al., Forecast skill of the Madden-Julian Oscillation in two Canadian atmospheric models, submitted to *Monthly Weather Review*, 2008); (2) MJO has apparently seasonal variation, characterized by a latitudinal migration across the equator between boreal winter and summer [*Zhang and Dong*, 2004]. The seasonality in the MJO is pronounced in zonal winds at the surface and low level (850 hPa) and precipitation. Figures 3 and 4 are obtained in the sense of statistics, and do not preclude the possibility that MJO activity has maximum variance over the equator at months such as spring or fall; (3) There is always relatively large amplitude in the near-equatorial western Pacific in Figures 3 and 4, which may excite downwelling Kelvin waves that propagate eastward and warm the eastern Pacific. All these MJO features are important to help understand MJO-ENSO connection as discussed in following sections.

[22] Figure 5 displays the recovered signal from the first CEOF mode, obtained by taking the real part of the product of the first CEOF complex eigenvector multiplied by the corresponding time series, for zonal winds and OLR, respectively. A short period from 1987–1991 was randomly chosen here for a clear presentation as in *Zavala-Garay et al.* [2005]. Figure 5 shows a pronounced MJO property, namely an apparent disturbance propagating eastward from the western to the central and then the eastern Pacific Ocean. In the following sections, we will use the first mode of CEOF to represent the MJO activity as in some other studies [e.g., *Zavala-Garay et al.*, 2005; Tang and Yu, submitted manuscript, 2008]. In particular, we define the MJO index by the temporal amplitude function of the first CEOF mode, which depicts the temporal evolution of the strength of MJO activity.

5. MJO-ENSO Relationship

[23] In this section, we will explore the MJO-ENSO relationship, with emphases on its nonlinear, seasonal and decadal dependence.

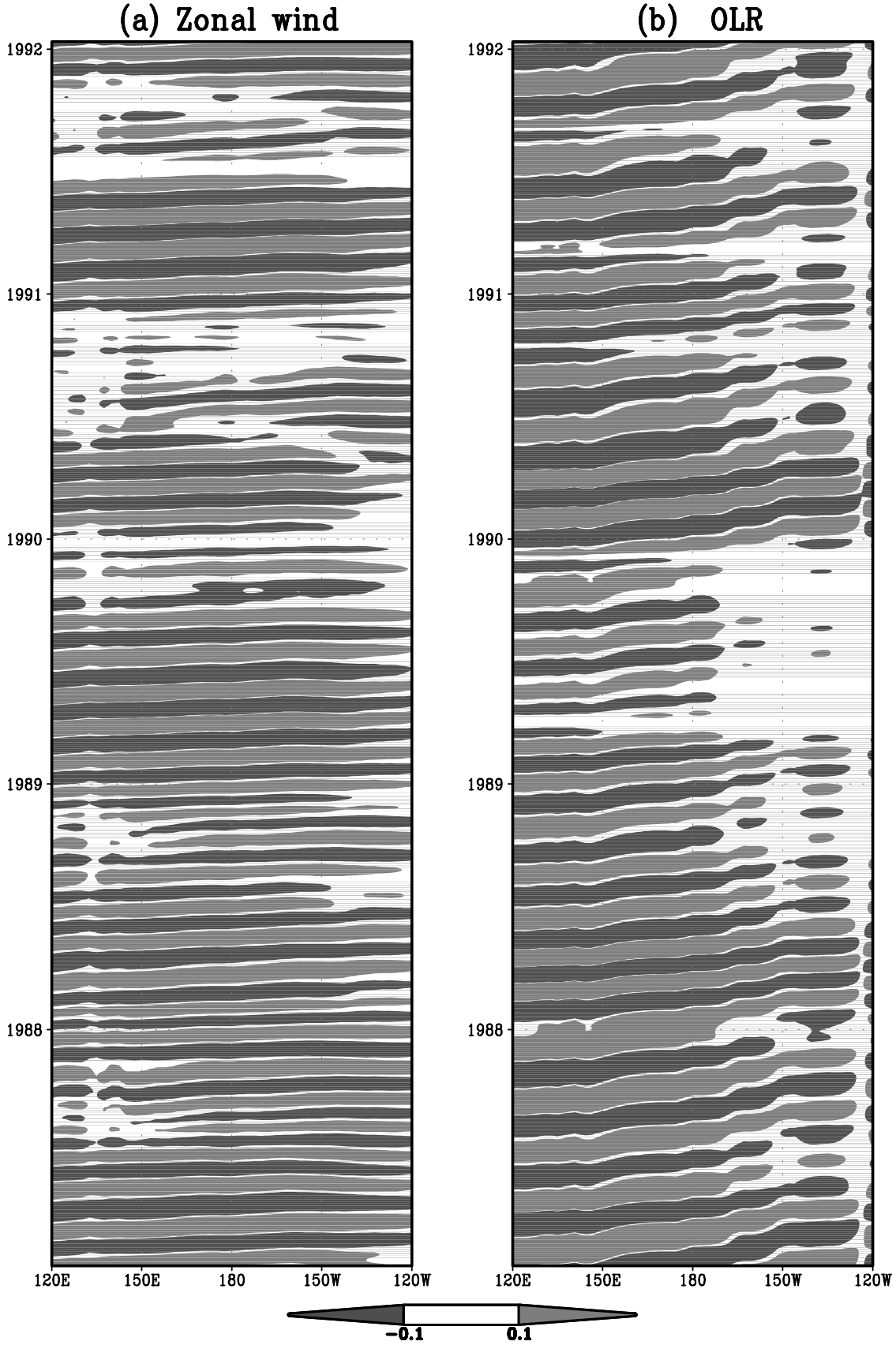

Figure 5. Time-longitude section of the recovered MJO signal using the first CEOF mode along 10°S for (a) zonal winds and (b) OLR.

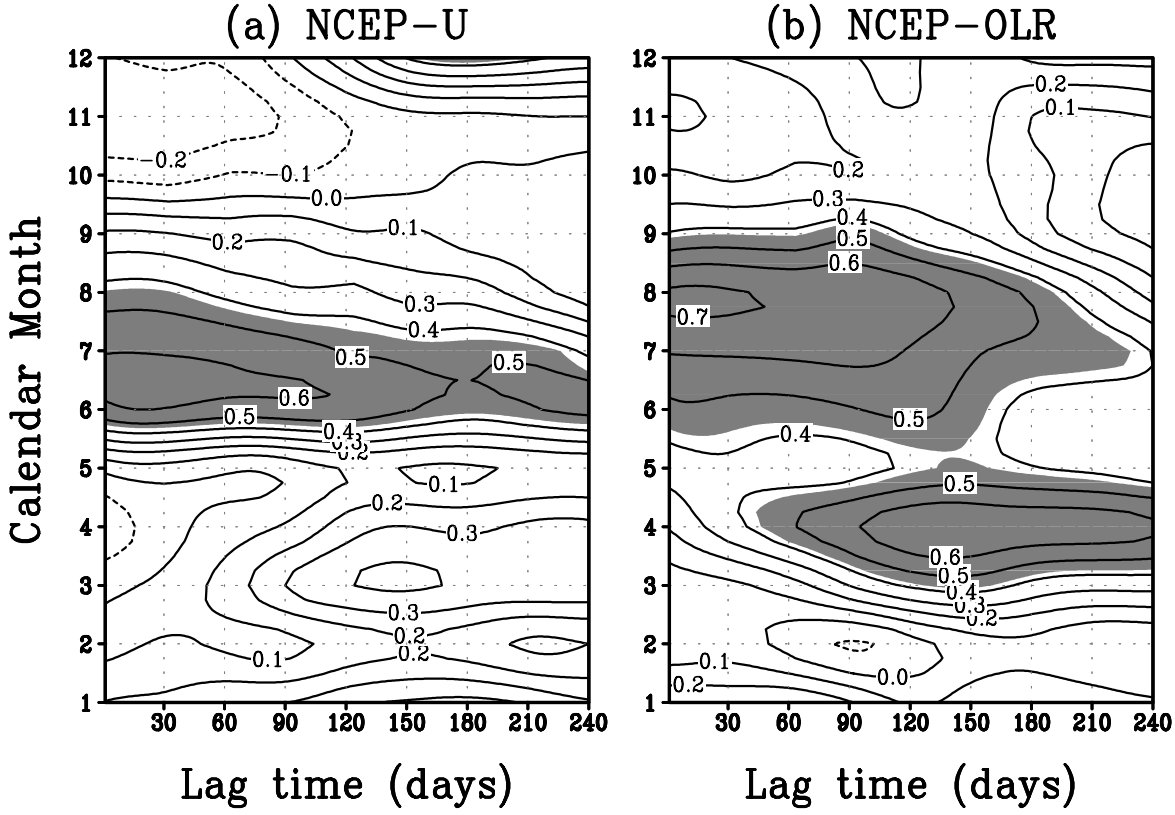

Figure 6. Lagged correlation of MJO indices, as functions of lag time (d) and start month, with Niño3 index. Shaded is the correlation that is statistically significant at a confidence level of 95%.

5.1. Nonlinearity of MJO-ENSO Relationship

[24] A conventional MJO index is usually defined as leading PCs (principal components) of one or multiple fields (e.g., zonal winds or OLR). It has been shown that with such a kind of MJO index, there is no statistically significant relationship between MJO and ENSO [e.g., *Slingo et al.*, 1999; *Hendon et al.*, 1999; *Kessler*, 2001]. On the other hand, recently *Hendon et al* [2007] and *McPhaden et al.* [2006] found that the relationship of MJO and ENSO varies with the season. Using the MJO index defined by the amplitude of leading PCs of the combined fields of zonal winds at 850 hPa, 200 hPa and OLR, they obtained significant correlation between boreal spring MJO activity and the subsequent autumn/winter ENSO variability. Their work differs from previous studies in two aspects. The first is the MJO index itself. The amplitude function they used is essentially a quadratic form of conventional PCs, therefore its linear correlation with ENSO could be viewed as equivalent to a nonlinear relationship of a PC-defined MJO index onto ENSO. The second is that they computed lagged correlation between MJO and ENSO indices only using data of some seasons. It was found that the MJO-ENSO relationship is far less significant when the data from all seasons were used [*Hendon et al.*, 2007]. Mathematically such a seasonal-dependent relationship could be described by a step function (nonlinear), namely good linear relationship in some seasons and no linear relationship in other seasons. Thus the overall relationship of MJO-ENSO is nonlinear in nature. This might explain the reason why some of previous studies failed to identify significant relationship of MJO-ENSO when only linear components were considered. Indeed, the MJO and ENSO are dominant atmospheric and oceanic variability with different timescales, thus their relationship, if existed, is most likely nonlinear.

[25] The evidence for the nonlinearity of MJO-ENSO relationship can be further demonstrated by correlating Nino3 index with conventional PC-defined MJO indices of zonal winds at the surface and OLR. The result shows that there is no significant correlation between the MJO and ENSO at all lags, even though the seasonal dependence is considered as discussed by *Hendon et al.* [2007] (not shown). This is consistent with earlier studies reported by *Slingo et al.* [1999] and *Hendon et al.* [1999].

[26] Another work to examine the nonlinearity of MJO-ENSO relationship was documented by Tang and Yu [submitted manuscript, 2008], where a nonlinear canonical correlation analysis (NLCCA) based on neural network was applied to PC-defined MJO index and ENSO index. With such a nonlinear statistical technique, a significant nonlinear correlation between MJO and ENSO can be identified, even though the seasonal dependence is not considered, namely samples of all seasons were used.

[27] Therefore a key issue in studying MJO-ENSO relationship is to consider its nonlinearity, such as employing either data of some seasons (years) with conventional linear methods or data of all seasons (years) with nonlinear statistical methods. In this study, we will focus on the former. The time amplitude function of the first CEOF mode of zonal winds or OLR will be used as the MJO

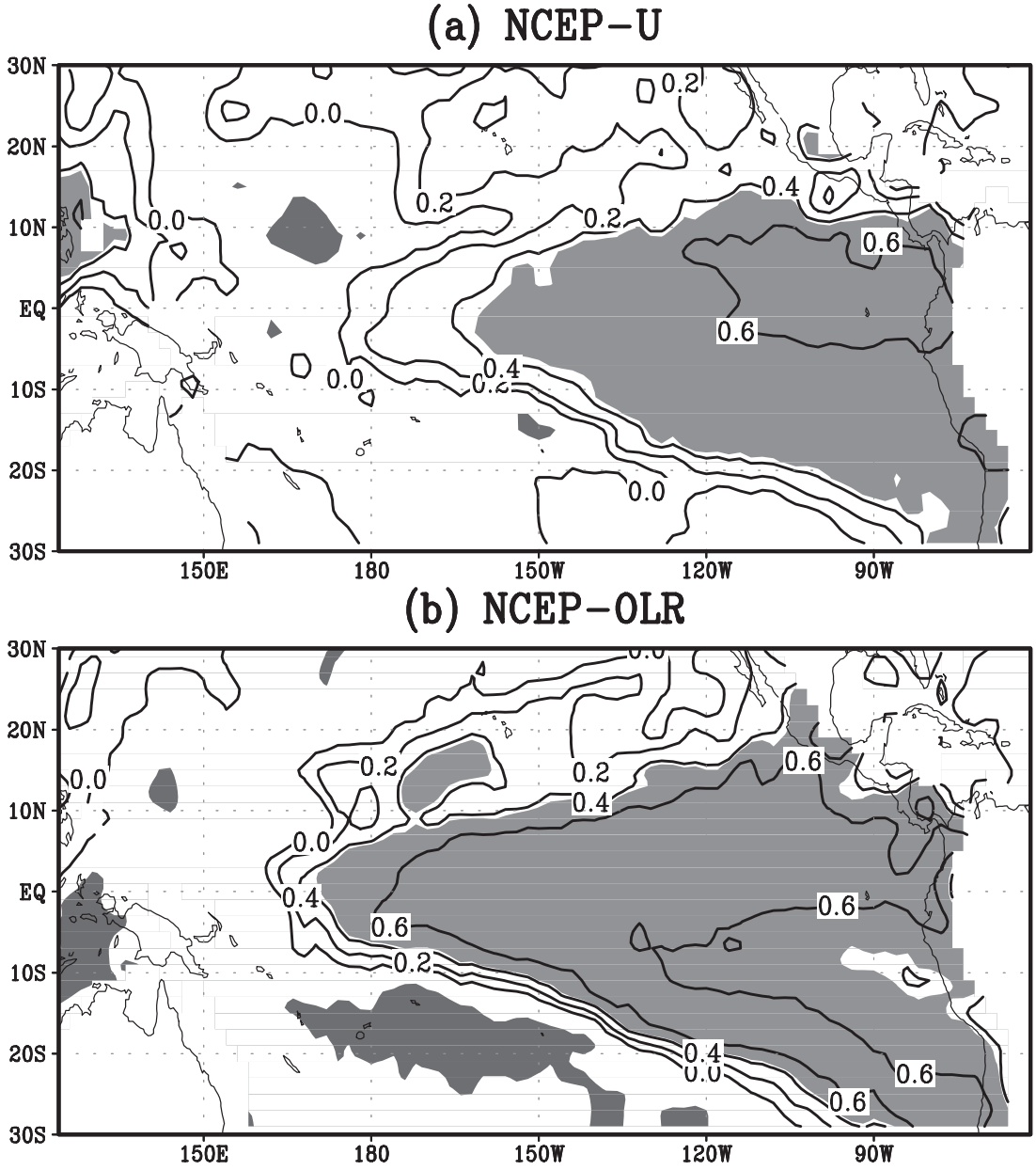

Figure 7. Correlation between MJO indices in July and SSTA in the subsequent October. Shaded is the correlation that is statistically significant at a confidence level of 95%.

index, as discussed in section 4. We will refer to these amplitude time series, with daily sampling, as MJO_U or MJO_{OLR}. These indices are different from the index used by *Hendon et al.* [2007] and *McPhaden et al.* [2006] where a 90-d running mean was applied prior to computing correlation. That might bring concerns since a 90-d running mean could remove signal of the period under 90 d.

5.2. Seasonal Dependence of MJO-ENSO Relationship

[28] We first use all data samples to calculate lagged correlation between MJO and Nino3 indices. As expected, the correlation is very small for all lags from 0 to 240 d (not shown). As argued by *Hendon et al.* [2007], the low correlation is the consequence of using all data samples. In fact, as we will see in following analyses, weak correlations in some seasons would greatly bias strong correlations in other seasons.

[29] Shown in Figure 6 is the lagged correlation function with lag time (abscissa) and start month (ordinate). The lag time is defined, unless otherwise indicated, by the time that MJO proceeds ENSO in this study. The lagged correlation was computed using the daily MJO index and the daily Niño3 (90°W to 150°W and 5°S to 5°N) SSTA index for the period from 1 January 1981 to 31 December 2003, and then averaged over calendar months. The correlation obtained by this means is almost identical to that computed using monthly data. Shaded in Figure 6 are regions where the correlation is statistically significant at the confidence level of 95% by two-tailed Student's t test (The number of degrees of freedom is estimated using the method intro-

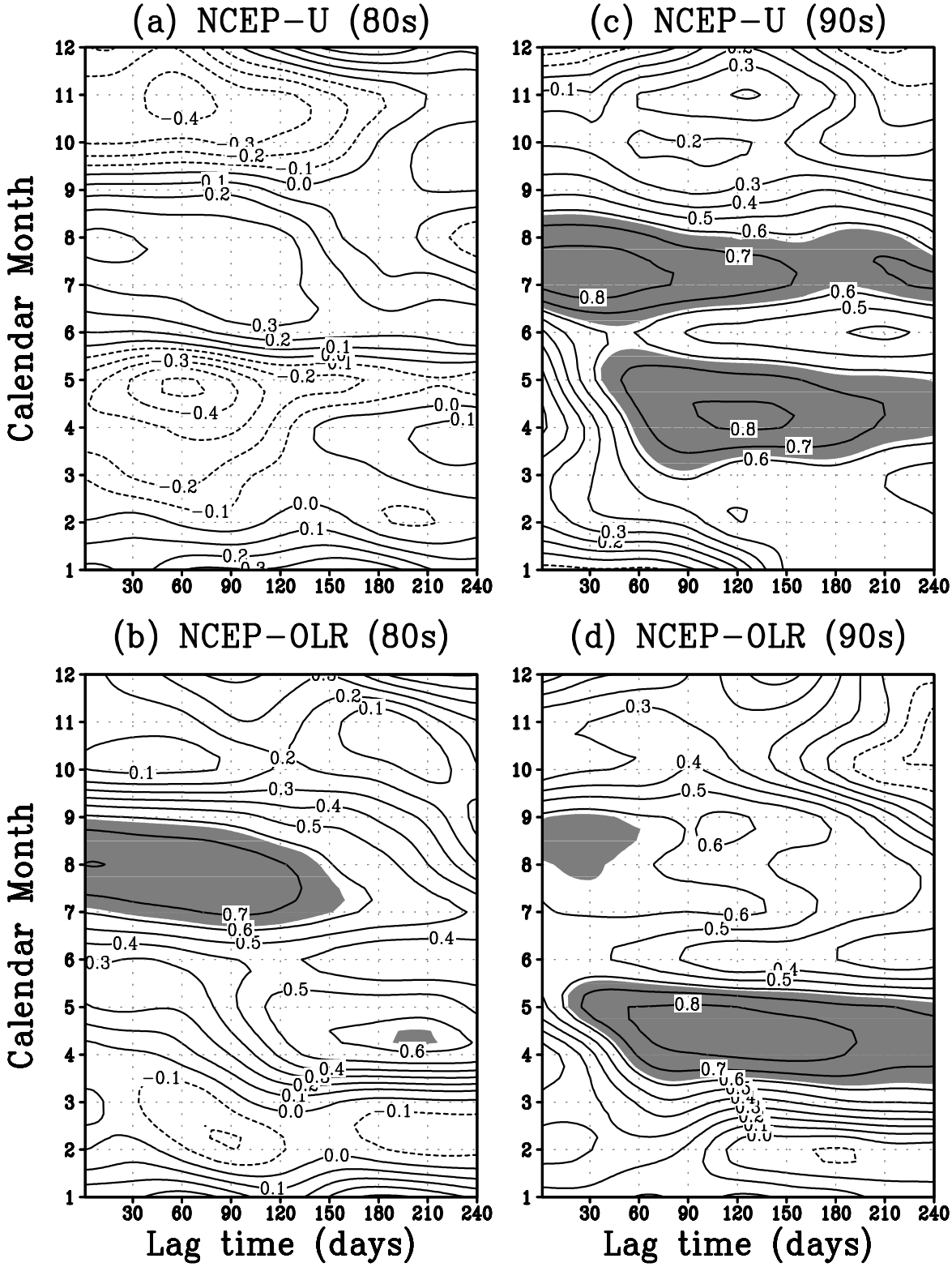

Figure 8. Same as Figure 6 but for correlations that are computed using the data during the period of (left) 1980s and (right) 1990s respectively.

duced in *Emery and Thomson* [1998], namely, $N_{eff} = \frac{N}{\sum_{l=-L}^{L}\left[r_{xx}(l)r_{yy}(l)+r_{xy}(l)r_{yx}(l)\right]}$ where, $r_{..}(l)$ is the lagged correlation coefficient at a time lag of l, and x and y denote SSTA and MJO indices repectively. L is the maximum lag, set to $N/3$ here, and N is the original sample size. Unless otherwise indicated, the method is always used in following statistical tests.).

[30] Figures 6a and 6b show both MJO_U and MJO_{OLR} in boreal summer significantly correlating with Niño3 SSTA

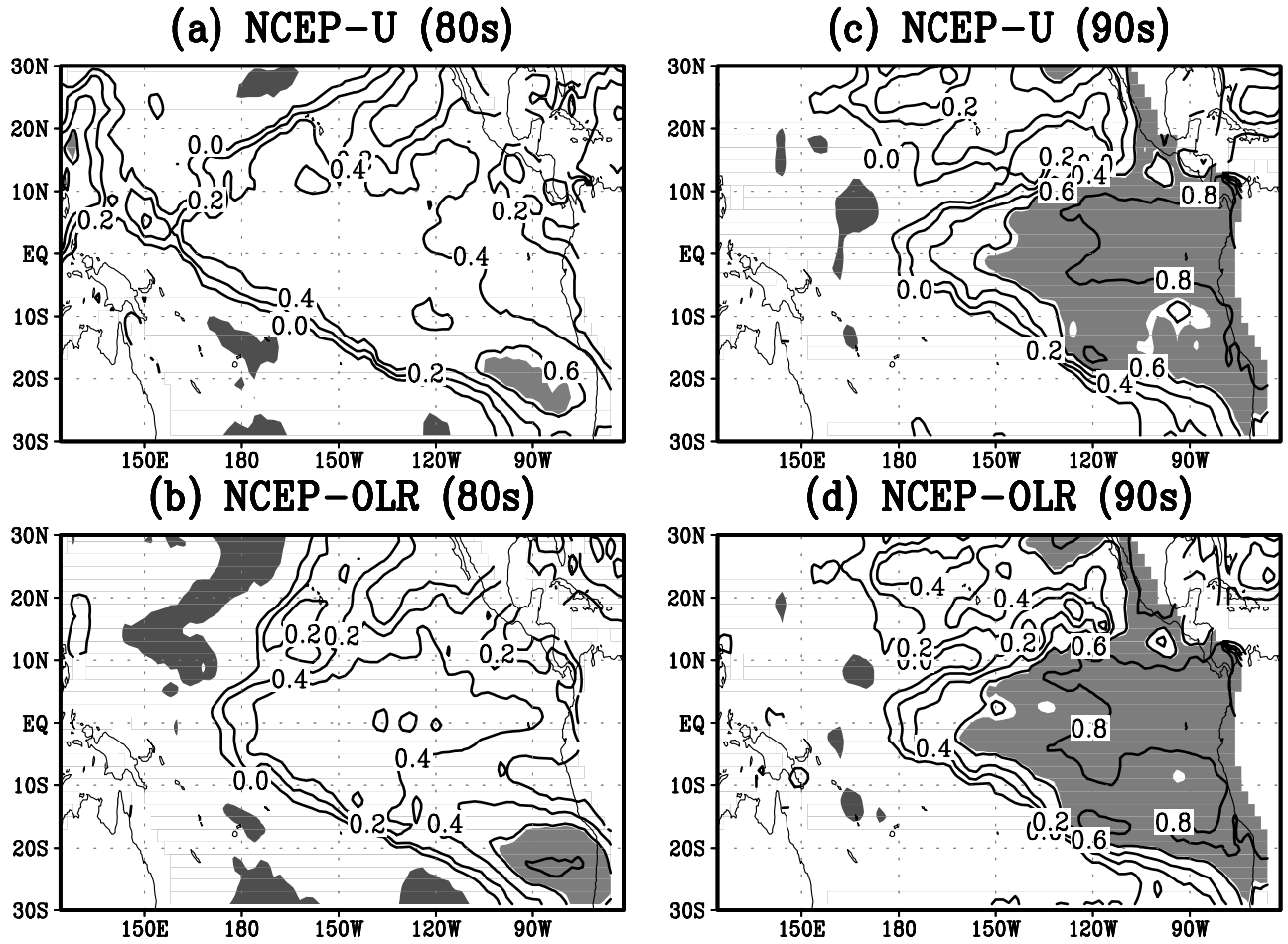

Figure 9. The correlations between the MJO indices in May with SSTA in the subsequent October. Shaded is the statistically significant correlation at the confidence level of 95%. The correlation was respectively computed for (a and b) the 1980s and (c and d) the 1990s.

several months later. Also MJO_{OLR} in boreal spring has a strong lagged relationship with Niño3 SSTA in the subsequent autumn-winter. Similar results were also obtained by *Hendon et al.* [2007], though they used a different MJO index.

[31] Figure 7 displays the correlation of MJO_U and MJO_{OLR} in July onto the tropical Pacific SSTA in the subsequent October. As can be seen, statistically significant correlation regions cover the whole tropical eastern Pacific like an El Niño pattern (shaded area). In addition, the MJO_{OLR} produced more marked correlations with SSTA than MJO_U. Results from the correlations between MJO_{OLR} in May and SSTA in October show a similar feature (not shown).

[32] The MJO activity is generally the strongest in boreal winter with the maximum variance occurring south of the equator in zonal winds at the surface and OLR, and a secondary maximum occurring north of the equator in boreal summer. The strong MJO activity near the equator tends to occur in boreal spring-early summer [*Zhang and Dong*, 2004]. One possible mechanism responsible for the connection of MJO-ENSO is through oceanic Kelvin waves. In an active MJO scenario, accompanying the eastward propagating MJO activity, large westerly wind anomalies bring warm water present in the central equatorial and eastern Pacific, which yields the warm SST and heat content (HC) anomalies in this region. A strong zonal HC gradient at the central equatorial Pacific weakens the upwelling there and intensifies the warm Kelvin waves propagating eastward. The warm eastward propagating Kelvin waves bring warm waters to the eastern Pacific Ocean to further intensify the anomalies, leading to positive SST anomaly in the east. It has been found that there exists a significant relationship between the MJO-driven Kelvin waves and the strength of El Niño, with the Kelvin waves preceding El Niño by around 2–3 months [e.g., *Zhang and Gottschalck*, 2002], which is very close to the time lag of maximum corelation between MJO activity in summer and subsequent El Niño in autumn-winter as shown in Figure 6a.

[33] While the above hypothesis explains the connection of MJO in summer with ENSO in autumn-winter, it might be unable to interpret the connection of MJO in spring with ENSO in autumn-winter as shown in Figure 6b. This is because the lag time of the maximum correlation here is around 6 months, a timescale far larger than the time required for Kelvin waves across the Pacific basin. Another possible mechanism for MJO-ENSO relationship is based on Bjerknes theory of trade wind, first proposed by *Bjerknes* [1969] and recently addressed by some researchers [e.g.,

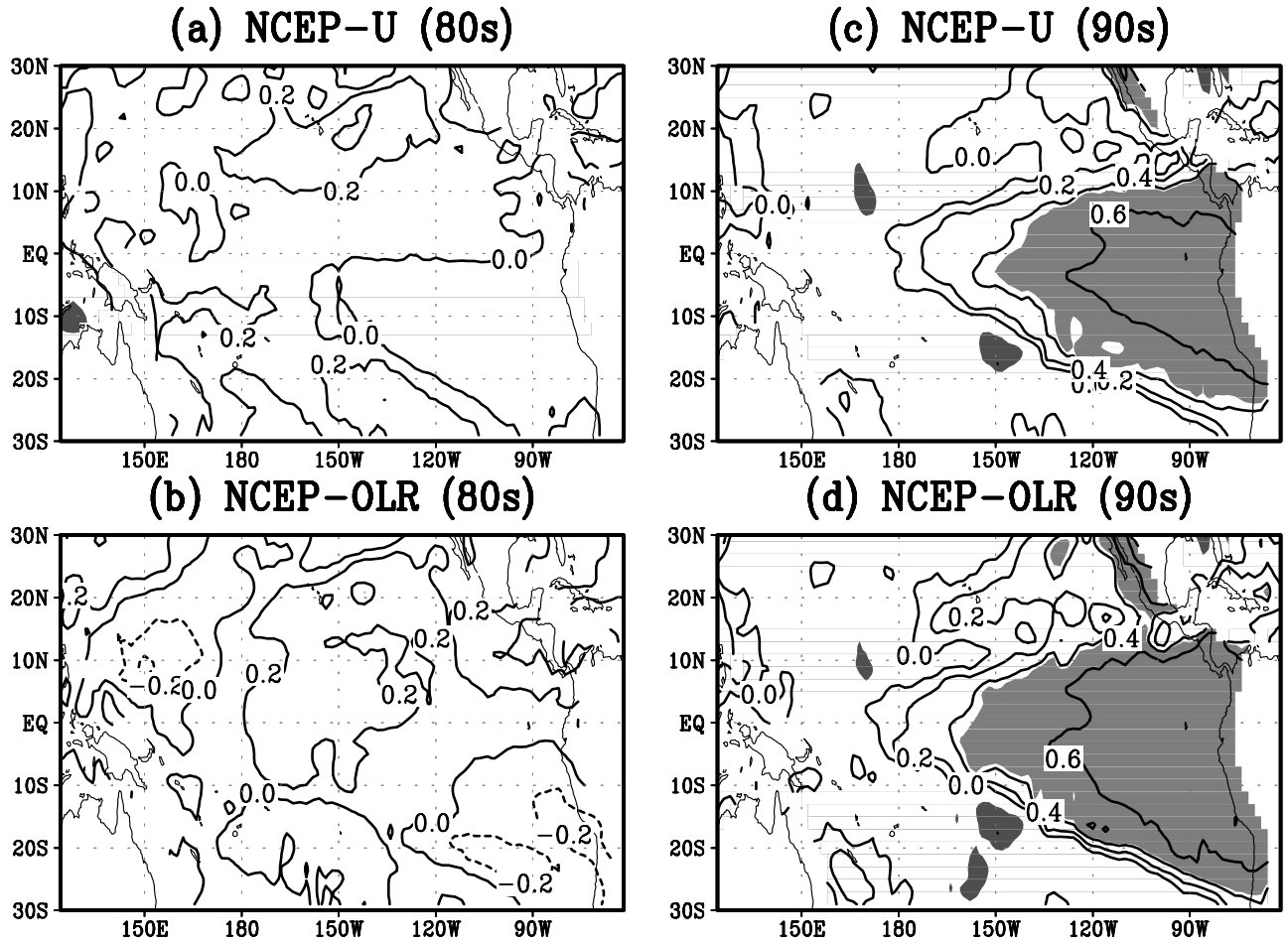

Figure 10. Same as Figure 9 but for the correlations between MJO in March−May and the tropical SSTA in the subsequent October−December.

Hendon et al., 2007; *Kessler and Kleeman*, 2000]. The core component here is the interaction between MJO-induced westerly anomalies with SST anomalies. It has been found that enhanced MJO activity often results in anomalous westerly surface winds in the western Pacific [e.g., *Kessler and Kleeman*, 2000; *Zavala-Garay et al.*, 2005]. In general, the westerly anomalies in the western Pacific preceed the development of El Niño through bringing surface warm water into the central and eastern Pacific. This process often starts in Spring. The warm water in the central and eastern Pacific enhances the SST zonal gradient there, and in turn intensifies westerly anomalies. Such a positive feedback between the westerly anomalies and SSTA in the central and eastern Pacific promotes enhanced MJO activity in the western Pacific, which then promotes enhanced surface westerlies in the western Pacific. These are highly conductive to El Niño conditions 6-8 months later as evidenced and argued by *Hendon et al.* [2007].

5.3. Decadal Dependence of MJO-ENSO Relationship

[34] A clear contrast in terms of the characteristics of the interannual variability exists between the 1980s and the 1990s in the Pacific ocean, evidenced by many observations such as sea level pressure, SST, low-level zonal wind, and subsurface ocean heat content anomalies [e.g., *Kleeman et al.*, 1996; *Tang and Hsieh*, 2002]. It is of interest to explore the impact of decadal variation of the interannual variability on MJO-ENSO relationship. Shown in Figure 8 are lagged correlations calculated using the data during 1981−1990 and 1991−2000 respectively. The lagged correlations between MJO and ENSO as noted in section 5.2 are more pronounced in the 1990s as compared to that in the 1980s, especially for MJO_U. Such a decadal variation of MJO-ENSO relationship can be further demonstrated in Figure 9, showing the correlation between MJO in May and the tropical SSTA in the subsequent October. As can be seen, the correlation displays an ENSO-like pattern for both decades with relatively large values occurring in the tropical eastern Pacific Ocean, whereas the correlation is less pronounced in the 1980s but more marked in the 1990s.

[35] To examine the impact of finite sample size on correlation coefficients in Figures 8 and 9, we calculated the correlation between MJO in March−May and the tropical SSTA in the subsequent October−December as shown in Figure 10. As such, the sample size is three times as much as that used in Figure 9 (However it does not mean the effective number of degree of freedom increases three times due to serial correlation existing in ENSO index. Instead, the effective number of degree of freedom increases from 10 to 21). Figure 10 is very similar to Figure 9, further suggesting that the impact of MJO on ENSO is weaker in the 1980s than in the 1990s.

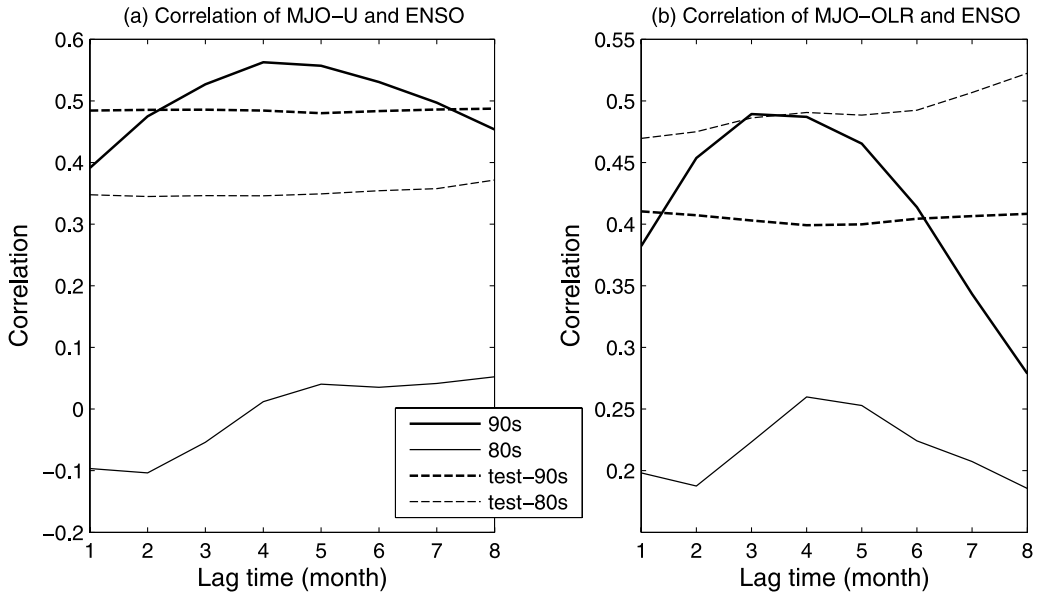

Figure 11. The lagged correlation between MJO and Nino3 SSTA indices, computed for the 1980s and the 1990s respectively. The correlation for the MJO_U index is shown in Figure 11a and for the MJO_{OLR} in Figure 11b. The bold-solid line is for the 1990s and thin-solid line for the 1980s. The statistically significant test is shown in dashed line, with bold-dashed line for the 1990s and thin-dashed line for the 1980s.

[36] Figure 11 shows the MJO-ENSO correlations in the 1980s and 1990s, calculated using data of all seasons. A striking decadal variation is clearly seen for both MJO_U and MJO_{OLR} indices. Statistical tests indicate that the MJO-ENSO correlation is significant at lags of 2–6 months for the 1990s at the 95% confidence level, but not significant at all lags for the 1980s. Figure 12 further compares MJO and ENSO indices for the period from 1981–2000. As expected, relatively strong MJO signal could be seen prior to several EL Niño events. Such a lagged relationship is more visible in the 1990s. For example, the MJO activity was strong before 1997 El Niño, but weak or absent prior to 1982 warm event. On the other hand, there were more "false alarms" in the 1980s, namely strong MJO activities do not lead to EL Niño events.

[37] It should be noticed that the decadal variation of MJO-ENSO relationship is not dependent on the MJO indices used in this study. To address this, we repeated the above analyses but used BMRC (Bureau of Meteorology of Research Center, Australia) MJO index (http://www.bom.gov.au/bmrc/clfor/cfstaff/matw/maproom/index.html), which was developed by *Wheeler and Hendon* [2004] and has been used in many MJO studies [e.g., *McPhaden et al.*, 2006; *Hendon et al.*, 2007]. Significant differences of MJO-ENSO relationship between the 1980s and 1990s are also striking as shown in Figures 13 and 14.

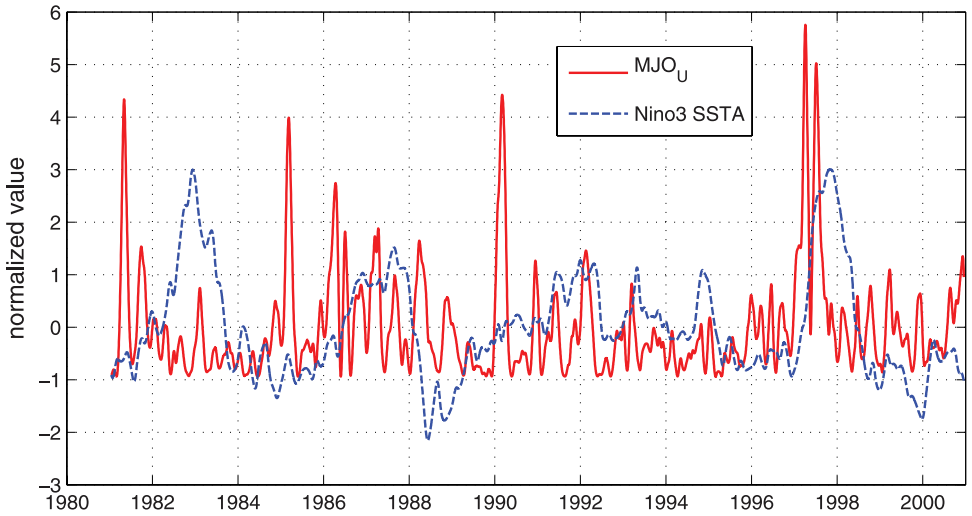

Figure 12. Normalized MJO and Nino3 indices from 1981–2000.

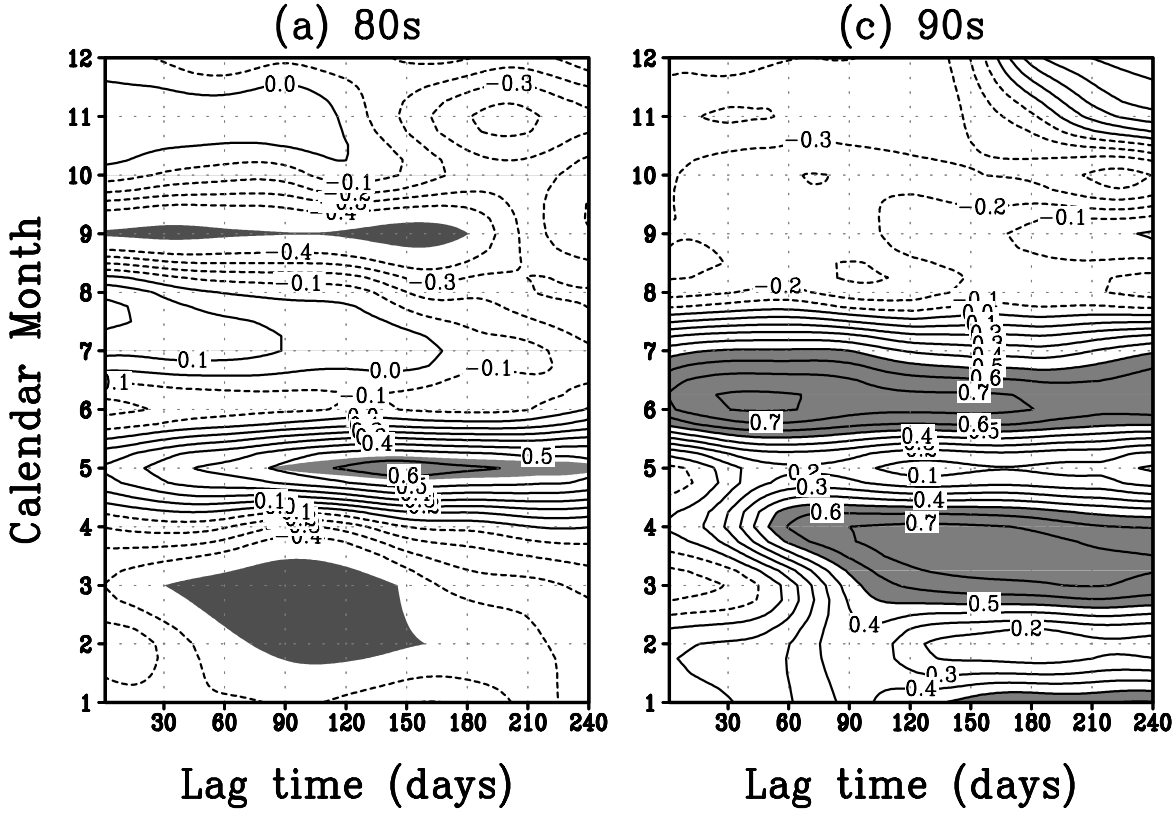

Figure 13. Same as Figure 8 but for the BMRC MJO index.

In addition, compared with Figures 8a and 13a also shows some marginally significant MJO-ENSO correlations in the 1980s, though far less pronounced compared with the correlation in the 1990s.

[38] The decadal variation of MJO-ENSO relationship is probably associated with the variation of both atmospheric anomalies (such as MJO wind anomalies) and ocean anomalies (SSTA) in the two decades. Shown in Figure 15 are the first EEOF modes of zonal winds, derived using the data of 1980s and 1990s respectively. Comparing the structure of EEOF modes between the two decades reveals that MJO has a period of around 50 d in the 1990s and 60 d in the 1980s, associated with a faster eastward shift of MJO activity and relatively stronger westerlies in the 1990s. As discussed in the above section, the impact of MJO on ENSO is most likely through the low-frequency westerly anomalies associated with enhanced MJO activity, which project efficiently onto the El Niño mode in spring [*Hendon et al.*, 2007]. Indeed, the observations show that the westerly wind is more prevailed over the equatorial western Pacific in the 1990s than in the 1980s [*Tang and Hsieh*, 2002]. The westerly anomalies over the equatorial western Pacific bring warm water to the central and the eastern Pacific, leading to El Niño conditions by either the downing Kelvin waves or the SST-westerly wind positive feedback as discussed above.

5.4. Further Verification of MJO-ENSO Relationship

[39] Based on the defined MJO indices, we have found significantly lagged correlations between MJO and ENSO. The MJO-ENSO relationship displays both seasonal and decadal dependence. These results were further confirmed using the BMRC MJO index. However, it is noted that the BMRC MJO index was also derived from NCEP-NCAR reanalysis product. In this subsection, the MJO-ENSO relationship is further examined using ECMWF ERA-40 reanalysis product.

[40] We repeated all analyses performed in sections 5.2 and 5.3 but used ECMWF ERA-40 to derive the MJO index. Similarly, the MJO index was defined by the amplitude function of the first CEOF. Correlating the ERA-40 MJO index with the tropical Pacific SSTA shows that the MJO-ENSO relationship reported above can also be obtained using the ERA-40 MJO index. Figure 16 is the lagged correlation of the ERA-40 MJO index with respect to the observed Niño3 SSTA index, as a function of lagged time and start month. Figures 16a–16c, highly resembling Figures 6a, 8a, and 8c, further verify the significant MJO-ENSO relationship obtained in proceeding sections. In addition, the lagged correlations of the ERA-40 MJO index in March–May onto the tropical SSTA in the subsequent October–December, as presented in Figure 17 for both the 1980s and the 1990s, also closely resemble Figure 10 obtained using the NCEP-NCAR reanalysis product. These indicate that the MJO-ENSO relationship identified in this study is not dependent on reanalysis products, though it is worth noting that the ECMWF and NCEP-NCAR reanalysis products are related each other somehow due to the same real observations used in their data assimilations.

6. Summary and Conclusion

[41] In this study, first, we analyzed the spatial and temporal characteristics of MJO using daily zonal winds

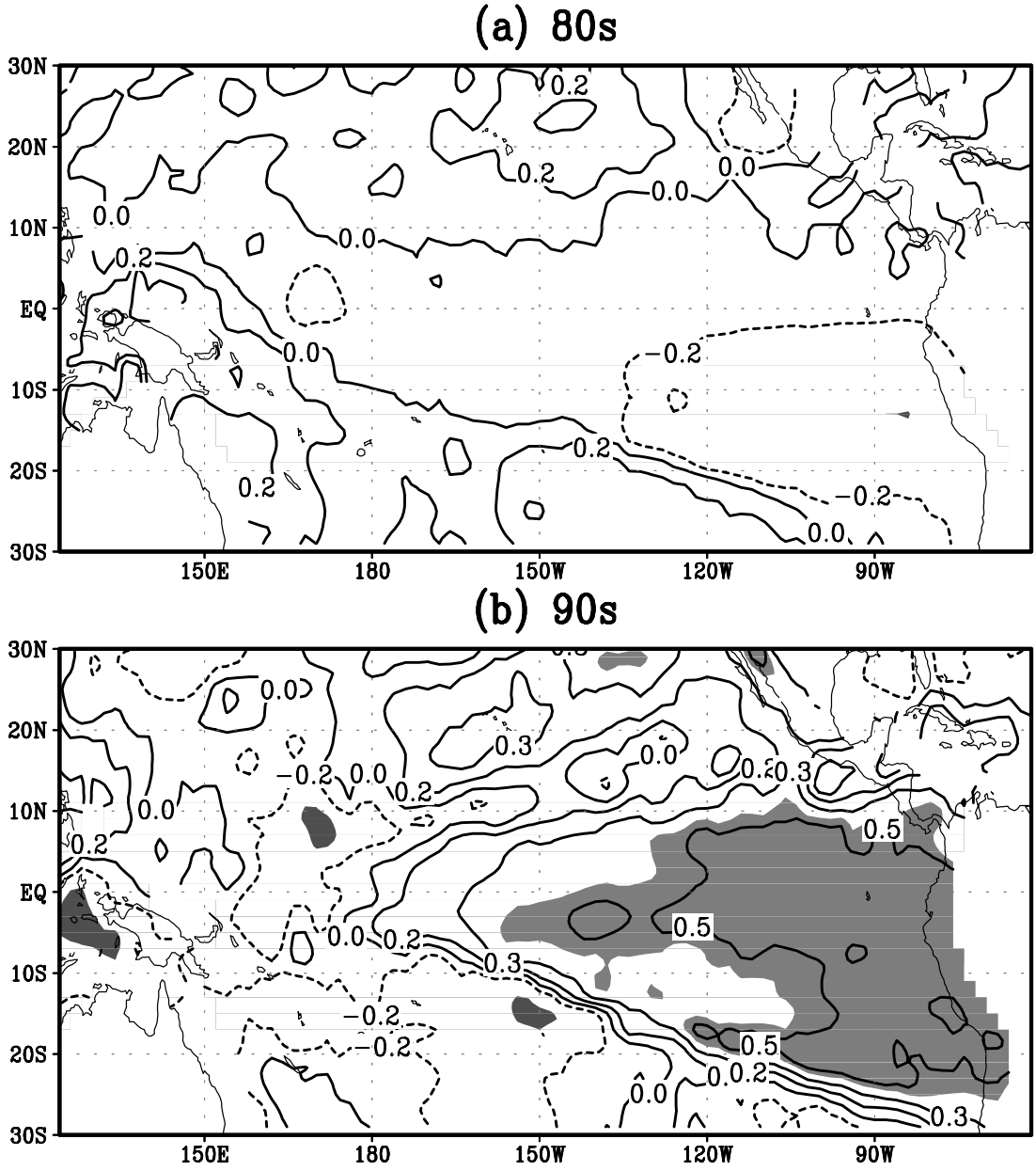

Figure 14. Same as Figure 10 but for the BMRC MJO index.

at the surface and OLR of NCEP-NCAR reanalysis product for the period from 1981–2003. Two estimates were made to detect MJO signals. The first estimate is based on the intraseasonally passed time series. In the second estimate, we removed the contribution of ENSO to MJO with aid of an empirical model. The two estimates show very similar features in terms of both MJO spatial structure and temporal variability. The ENSO contribution to MJO is subtle whereas MJO activity, represented in the two fields, mainly exists around 10° off the equator and over the near-equatorial western Pacific.

[42] We then focus on analyzing the MJO-ENSO relationship, the central issue addressed in this study. It has been found that there exists a significant relationship between MJO in spring–summer and ENSO in autumn–winter. Two possible mechanisms are responsible for this relationship. The relationship between MJO in summer and ENSO in autumn is probably related to the oceanic downwelling Kelvin waves, which are excited by eastward propagating MJO activity in the equatorial western Pacific. The eastward propagating Kelvin waves bring warm water present in the tropical central and eastern Pacific, which yields the warm SST anomalies. For the relationship between MJO in spring and ENSO in autumn–winter, a positive feedback between MJO-induced westerly anomalies and the SST anomalies appears to be a major passway. The anomalous westerly surface winds in the western Pacific associated with enhanced MJO activity bring surface warm water into the tropical central and eastern Pacific. The warm water enhances the SST zonal

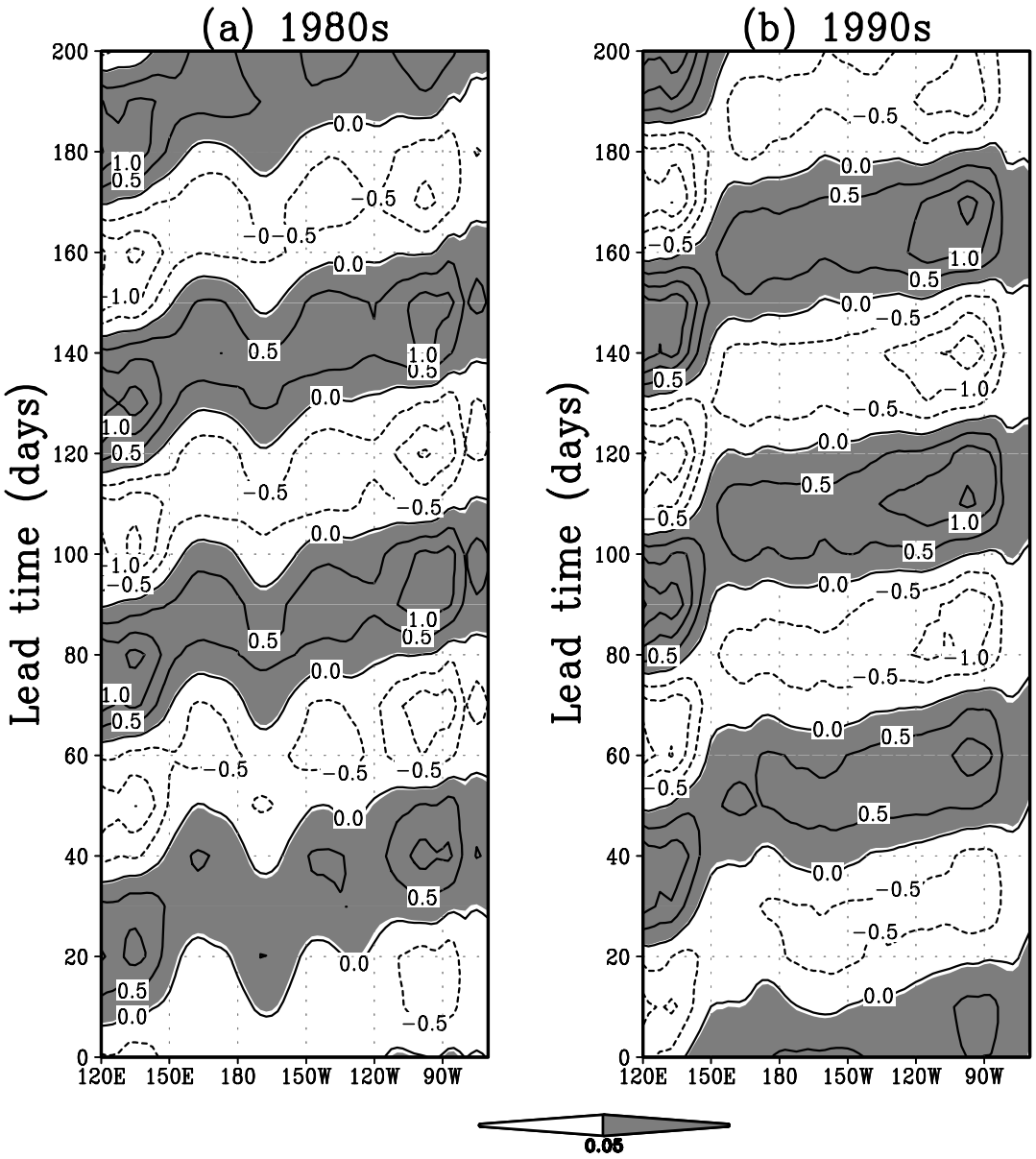

Figure 15. The first EEOF modes of NCEP reanalysis zonal winds for (a) 1980s and (b) 1990s. The unit is m s^{-1} and the contour interval is 0.5.

gradient there, and in turn intensifies westerly anomalies. The relationship between MJO in spring and ENSO in autumn-winter has also been addressed by *Hendon et al.* [2007].

[43] One new finding in this study is that MJO-ENSO relationship has decadal variation. The relationship between MJO in spring–summer and ENSO in autumn–winter is much more significant in the 1990s than in the 1980s. This is most probably due to the decadal variation of MJO activity and ENSO variability. It has been found that during the 1990s, the MJO activity appeared more frequent, and the westerly wind was more prevailed over the equatorial western Pacific. As discussed by *Hendon et al.* [2007], the impact of MJO on ENSO is most probably through the low-frequency westerly anomalies that are associated with enhanced MJO activity and project efficiently onto the El Niño mode in spring. The strong westerly winds drive warm water to the tropical central and eastern Pacific to strengthen the development of El Niño.

[44] Some cautions should be taken regarding the decadal variation of MJO-ENSO relationship reported here. First, the finite effective samples used for the analysis is a concern. There are only four and five ENSO events in the 1980s and the 1990s respectively. The correlation coefficient obtained using daily data has a sample size of around 300 in Figures 8 and 9 and 900 in Figure 10, however the effective number of degree of freedom is not as large due to the strong serial correlation in SST data. This might have an effect on the robustness of our results though statistical significance tests based on the effective number of degree of freedom was performed. Second the data itself might have a contribution to the decadal variation of MJO-ENSO relationship. During TOGA decade starting in 1985 many new oceanic observational systems were gradually put in place

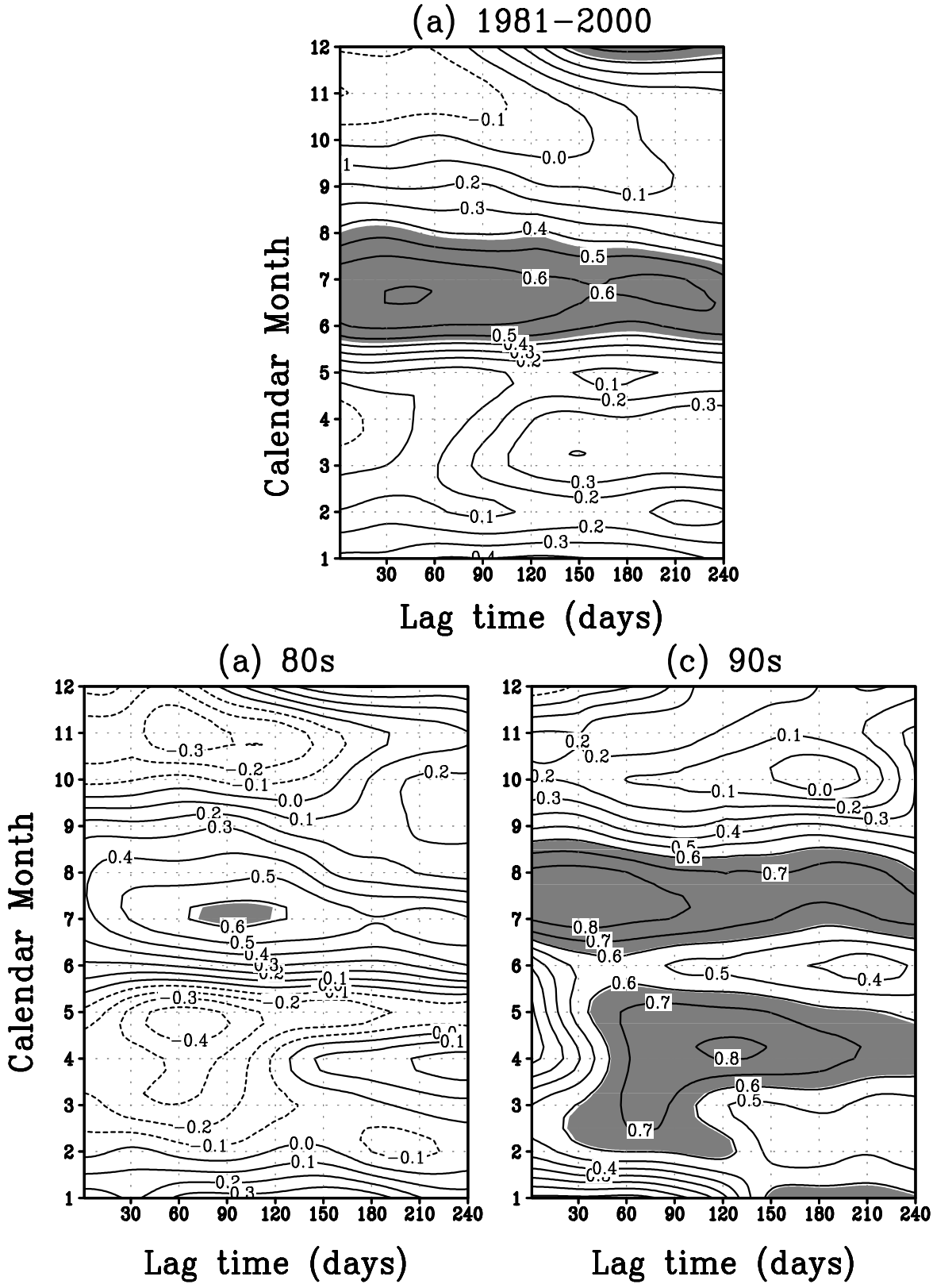

Figure 16. (a) Same as Figure 6a but for the MJO index that is derived from ECMWF ERA-40 reanalysis zonal winds at the surface. (b and c) Same as Figures 8a and 8c but for the ERA-40 MJO index.

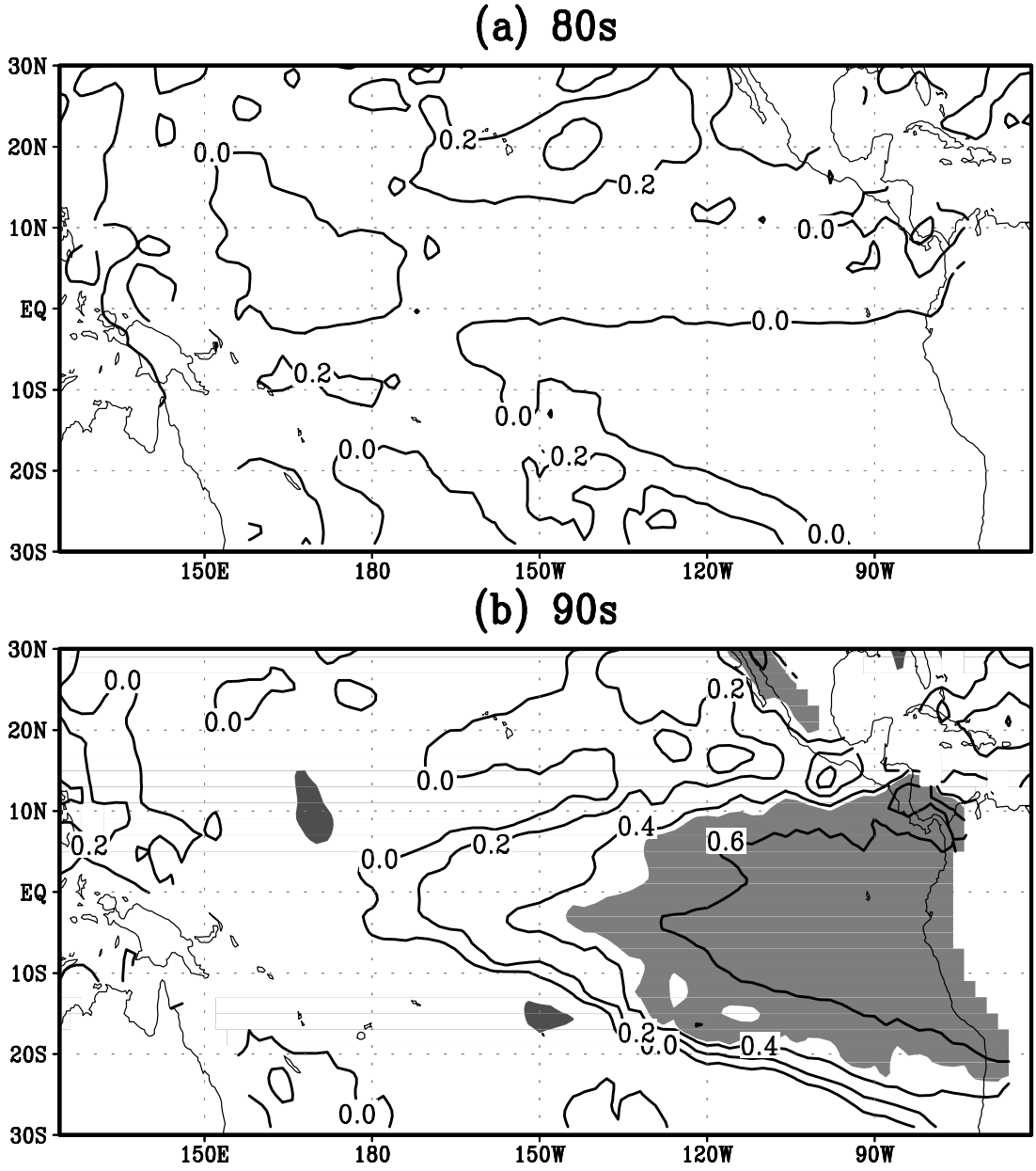

Figure 17. Same as Figure 10 but for the ERA-40 MJO index.

which would have added more accuracy to the reanalyzed surface winds in NCEP-NCAR and ER40 products. *McPhaden et al.* [2006] also found a better relationship between MJO and ENSO indices after 1995 when the TAO array observational system was completed and provided oceanic upper thermal field data. On the other hand, the significant difference of MJO-ENSO relationship also exists between the 1980s and the 1990s in OLR. It was believed that the additional surface data would probably have little impact on the OLR. Nevertheless, the present analysis is to date the first exploratory work to discuss possible decadal variation of MJO-ENSO relationship, which provides some insights into the impact of MJO on ENSO.

[45] This study is also able to shed some lights on ENSO mechanisms. Nonlinear dynamics and stochastically forcing linear dynamics are two most widely accepted candidates for ENSO mechanisms. Indeed, the role of stochastically forcing on ENSO cycle has been addressed at various times, especially since the late 1990s. A key issue in studying the impact of stochastic forcing on ENSO is to extract large-scale stochastic forcing patterns responsible for ENSO behavior. This can be implemented by a linear stochastic dynamical framework introduced by *Kleeman and Moore* [1997], i.e., stochastic optimal of coupled models. Many studies have shown that the stochastic optimal of a coupled model is the forcing pattern most favored to trigger ENSO-like oscillation [e.g., *Moore et al.*, 2006]. Since MJO is a dominant atmospheric intraseasonal mode and has a large spatial and temporal scale, one may be able to use MJO to represent the stochastic optimal to study the response of

ENSO to stochastical forcing. However, results from the present study also indicate that ENSO variability does not always rely on MJO forcing such as 1982 El Niño event where the MJO forcing was absent. A more detailed investigation requires sensitivity experiments of the response of ENSO to MJO, which is under the way.

[46] **Acknowledgments.** This work was supported by the Canadian Foundation for Climate and Atmospheric Sciences through its network of Global Ocean-Atmosphere Prediction and Predictability (GOAPP) and Canada Research Chair program. We thank three anonymous reviewers for their comments on the improvements of this paper.

References

Barnett, T. P. (1983), Interaction of the monsoon and Pacific trade wind system at interannual time scales. part I: The equatorial zone, *Mon. Weather Rev.*, *111*, 756–773.

Bjerknes, J. P. (1969), Atmospheric teleconnections from the equatorial Pacific, *Mon. Weather Rev.*, *97*, 163–172.

Blanke, B., J. D. Neelin, and D. Gutzler (1997), Estimating the effect of stochastic wind stress forcing on ENSO irregularity, *J. Clim.*, *10*, 1473–1486.

Bretherton, C. S., C. Smith, and J. M. Wallace (1992), An intercomparison of methods for finding coupled patterns in climate data, *J. Clim.*, *5*, 541–560.

Eckert, C., and M. Latif (1997), Predictability of a stochastic forced hybrid coupled model of El Niño, *J. Clim.*, *10*, 1488–1504.

Emery, W. J., and R. E. Thomson (1998), *Data Analysis Methods in Physical Oceanography*, p. 400, Elsevier, New York.

Harrison, E. D., and B. S. Geise (1991), Episodes of surface westerly winds as observed from islands in the western tropical Pacific, *J. Geophys. Res.*, *96*, 3221–3237.

Hasselmann, K. F. (1976), Stochastic climate models. part I: Theory, *Tellus, Ser. A and Ser. B*, *28*, 473–484.

Hendon, H. H., C. Zhang, and J. Glick (1999), Interannual variation of the Madden-Julian oscillation during austral summer, *J. Clim.*, *12*, 2538–2550.

Hendon, H. H., M. Wheeler, and C. Zhang (2007), Seasonal dependence of the MJO-ENSO Relationship, *J. Clim.*, *20*, 531–543.

Kessler, W. (2001), EOF Representations of the Madden-Julian Oscillation and its connection with ENSO, *J. Clim.*, *14*, 3055–3061.

Kessler, W. S., and R. Kleeman (2000), Rectification of the Madden-Julian Oscillation into the ENSO cycle, *J. Clim.*, *13*, 3560–3575.

Kleeman, R., and A. M. Moore (1997), A theory for the limitation of ENSO predictability due to stochastic atmospheric transients, *J. Atmos. Sci.*, *54*, 753–767.

Kleeman, R., R. Colman, N. R. Smith, and S. B. Power (1996), A recent change in the mean state of the Pacific Ocean: Observational evidence, atmospheric and oceanic responses, *J. Geophys. Res.*, *101*, 20,483–20,499.

Lau, K. M., L. Peng, T. Nakazawa, and C. H. Sui (1989), Dynamics of super cloud clusters, westerly wind bursts, 30–60 day oscillations and ENSO - An unified view, *J. Meteorol. Soc. Jpn.*, *67*, 205–219.

McPhaden, J. M. (1999), Genesis and evolution of the 1997–98 El Nino, *Science*, *283*, 950–954.

McPhaden, J. M., X. Zhang, H. Henden, and C. Wheeler (2006), Large scale dynamics and MJO forcing of ENSO variability, *Geophys. Res. Lett.*, *33*, LI6702, doi:10.1029/2006GL026786.

Moore, A., and R. Kleeman (1999), Stochastic forcing of ENSO by the Intraseasonal Oscillation, *J. Clim.*, *12*, 1199–1220.

Moore, A. M., J. Zavala-Garay, Y. Tang, R. Kleeman, A. T. Weaver, J. Vialard, K. Sahami, and D. L. T. Anderson (2006), Optimal forcing patterns for coupled models of ENSO climate, *J. Clim.*, *19*, 4683–4699.

Reynolds, R. W., and T. M. Smith (1994), Improved global sea surface temperature analysis using optimal interpolation, *J. Clim.*, *7*, 929–948.

Slingo, J. M., D. B. Rowell, K. R. Sperber, and F. Nortley (1999), On the predictability of the inner annual behavior of the Madden-Julian Oscillation and its relationship with El Niño, *Q. J. R. Meteorol. Soc.*, *125*, 583–609.

Tang, Y., and W. W. Hsieh (2002), Hybrid coupled models of the tropical Pacific–ENSO prediction, *Clim. Dyn.*, *19*, 343–353.

Tang, Y., W. W. Hsieh, B. Tang, and K. Haines (2001), A neural network atmospheric model for hybrid coupled modeling, *Clim. Dyn.*, *17*, 445–455.

Tangang, F. T., B. Tang, A. H. Monahan, and W. W. Hsieh (1998), Forecasting ENSO events: A neural network-extended EOF approach, *J. Clim.*, *11*, 29–41.

Uppala, S. M., et al. (2005), The ERA-40 reanalysis, *Q. J. R. Meteorol. Soc.*, *131*, 2961–3012.

Webster, P. J., and T. N. Palmer (1997), The past and future of El Nino, *Nature*, *390*(12), 562–564.

Wheeler, M. C., and H. H. Hendon (2004), An all-season real-time multivariate MJO Index: Development of an index for monitoring and prediction, *Mon. Weather Rev.*, *132*, 1917–1932.

Yu, L., and M. Rienecker (1998), Evidence of an extratropical atmospheric influence during the onset of the 1997–98 El Nino, *Geophys. Res. Lett.*, *25*(18), 3537–3540.

Zavala-Garay, J., C. Zhang, A. Moore, and R. Kleeman (2005), On the linear response of ENSO to the Madden Julian Oscillation, *J. Clim.*, 2441–2459.

Zhang, C., and M. Dong (2004), Seasonality of the Madden-Julian Oscillation, *J. Clim.*, *17*, 3169–3180.

Zhang, C., and J. Gottschalck (2002), SST anomalies of ENSO and the Madden-Julian Oscillation in the equatorial Pacific, *J. Clim.*, *15*, 2429–2445.

Y. Tang, Environmental Science and Engineering, University of Northern British Columbia, 3333 University Way, Prince George, BC, Canada V2N 4Z9. (ytang@unbc.ca)

B. Yu, Climate Research Division, Environment Canada, 4905 Dufferin Street, Toronto, ON M3H5T4, Canada.